# Evolution of various initial many-particle configurations to disordered stealthy hyperuniform ground states

Samuel J. Dawley [1] and Salvatore Torquato [1,2,3,4,*]

[1]*Department of Chemistry, Princeton University, Princeton, New Jersey 08544, USA*
[2]*Department of Physics, Princeton University, Princeton, New Jersey 08544, USA*
[3]*Princeton Materials Institute, Princeton University, Princeton, New Jersey 08544, USA*
[4]*Program in Applied and Computational Mathematics, Princeton University, Princeton, New Jersey 08544, USA*

(Received 4 July 2025; accepted 17 September 2025; published 8 October 2025)

Systems of particles interacting via stealthy potentials, a family of soft, long-ranged, isotropic pair potentials, possess infinitely degenerate disordered hyperuniform classical ground states of fundamental and practical interest, highlighted by their novel optical and mechanical properties. The configurational dimensionality of the ground-state manifold depends on a dimensionless parameter $\chi$ that measures the number of independently constrained degrees of freedom in a ground state. Starting from a wide class of initial two-dimensional point configurations, we study the evolution of trajectories of the collective-coordinate optimization procedure to their corresponding disordered stealthy hyperuniform ground states as a function of $\chi$ within the disordered regime ($0 < \chi < 1/2$). Initial conditions studied span a wide class of disordered systems, including antihyperuniform, nonhyperuniform, and hyperuniform ones. The evolution of the trajectories is quantified by computing a translational order metric and configurational proximity metric as a function of the computational time for selected values of $\chi$ within the disordered regime. The rate at which trajectories approach the ground-state manifold is fastest for those evolved from hyperuniform states and slowest for those evolved from antihyperuniform states. We observe that ground-state ensembles with distinct pair statistics are sampled by different initial conditions across a broad range of $\chi$ and that these pair statistics are generally effected by higher-order spatial correlations characterizing the initial condition. Learning how to manipulate initial conditions in the optimization procedure to target different portions of the ground-state manifold enables one to explore structurally unique stealthy ground states with designed short- up to intermediate-ranged spatial correlations for the purposes of materials discovery.

DOI: 10.1103/9wbz-h7t4

## I. INTRODUCTION

Disordered hyperuniform systems are exotic states of matter that anomalously suppress infinite-wavelength normalized density fluctuations relative to those in ordinary liquids and structural glasses [1,2]. They arise in a variety of contexts, including but not limited to the spatial distribution of avian photoreceptors [3], the organization of antigen receptors in the immune system [4], maximally random jammed sphere packings [5–8], the distribution of eigenvalues in random matrices [9], fermionic ground states [10,11], nonequilibrium phase transitions [12–16], vortex distribution in superconductors [17,18], classical and quantum spin liquids [19], active matter [20,21], quasicrystals [22], multiscale order of the prime numbers [23], and the large-scale structure of the universe [24]. A hyperuniform system is one in which the structure factor $S(\boldsymbol{k})$ vanishes in the limit that the wave number $k \equiv |\boldsymbol{k}|$ goes to zero [25].

Stealthy hyperuniform systems, the focus of this paper, are a subclass of hyperuniform states in which $S(\boldsymbol{k}) = 0$ for a finite range of wave numbers $0 < k \leqslant K$ [26–28]. These unusual amorphous states of matter are endowed with novel structural and physical properties, including complete isotropic photonic [29–31] and phononic [32–34] band gaps, and favorable dielectric characteristics [35–38] and transport properties [39–42]. At low temperatures they are characterized by singular thermodynamic features, including negative thermal expansion [28,43,44]. Further, these materials serve as a platform for studying deep-subwavelength wave localization in disordered materials [45].

Disordered stealthy hyperuniform ground states are infinitely degenerate with a configurational dimensionality which depends on the density. In the simplest setting we consider a set of $N$ points at positions $\boldsymbol{r}^N \equiv \boldsymbol{r}_1, \ldots, \boldsymbol{r}_N$ within a $d$-dimensional fundamental cell $\Omega$ of volume $V_\Omega$ with periodic boundaries at number density $\rho$. Particles interact via a bounded, integrable, and radially isotropic pair potential $v(\boldsymbol{r})$ such that its Fourier transform $\tilde{v}(\boldsymbol{k})$ exists and is positive over the compact interval $0 \leqslant k \leqslant K$, deemed the "exclusion region," and zero otherwise [28]. The total potential is represented in Fourier space as

$$\Phi(\boldsymbol{r}^N) = \frac{N}{2V_\Omega}\left[\sum_{k\leqslant K}\tilde{v}(\boldsymbol{k})S(\boldsymbol{k}) - \sum_{k\leqslant K}\tilde{v}(\boldsymbol{k})\right], \tag{1}$$

*Contact author: torquato@electron.princeton.edu

 ©2025 American Physical Society

TABLE I. Two-dimensional point patterns used as initial conditions for collective-coordinate optimization. Systems include configurations derived from a random sequential addition (RSA) process, those with Gaussian pair statistics (GAU), uniformly randomized lattices [UR(S/T)L], ensembles of equilibrium hard disks at different volume fractions (EHD), a Poisson point process (POS), equiluminous point patterns (EQLS), and a hyperplane intersection process (HIP), all of which are defined in Sec. III. All systems consist of $N$ particles at number density $\rho = 1$ and cover a range of antihyperuniform, nonhyperuniform, and hyperuniform classes, which span various degrees of disorder across length scales. The number of particles for the HIP and RSA patterns represent ensemble-average values.

| Initial condition | Abbreviation | $N$ | Antihyperuniform | Nonhyperuniform | Hyperuniform |
|---|---|---|---|---|---|
| Hyperplane intersection process | HIP | 1021 | ✓ | — | — |
| Equiluminous point pattern (luminosity $I$) | $\text{EQLS}_I$ | 1024 | — | ✓ | — |
| Poisson point process | POS | 1024 | — | ✓ | — |
| Equilibrium hard disks (volume fraction $\phi$) | $\text{EHD}_\phi$ | 1024 | — | ✓ | — |
| Uniformly randomized (Square/Triangular) lattice | UR(S/T)L | 1024 | — | — | ✓ |
| Gaussian pair statistics | GAU | 1000 | — | — | ✓ |
| Saturated random sequential addition | RSA | 1005 | — | ✓ | — |

where summation includes all wave vectors $\boldsymbol{k}$ appropriate to $\Omega$. The structure factor is expressed in terms of the collective density variables $\tilde{n}(\boldsymbol{k})$ as

$$S(\boldsymbol{k}) = \frac{|\tilde{n}(\boldsymbol{k})|^2}{N}, \tag{2}$$

where the $\tilde{n}(\boldsymbol{k})$ are defined by coefficients in the Fourier series of the local number density:

$$\tilde{n}(\boldsymbol{k}) = \sum_{j=1}^{N} \exp\left(-i\boldsymbol{k}\cdot\boldsymbol{r}_j\right). \tag{3}$$

If particles are arranged such that $S(\boldsymbol{k})$ is driven to its minimum value of zero for all $\boldsymbol{k}$ within the exclusion region, then from Eq. (1) it is seen that the system must be at its global energy minimum, the classical ground state. Stealthy ground states can be obtained through collective-coordinate optimization, a reciprocal-space-based approach which searches for the global minimum of (1) via numerical minimization [26,46]. Numerically obtained configurations along the ground-state manifold can be found to within $\Phi < 10^{-22}$ of the global minimum at the level of double-double numerical precision of the zero of the machine [47,48]. GPU (graphical processing unit)-based algorithms can be used to find stealthy ground states within $\Phi < 10^{-46}$ of the zero of the machine to within quadruple-double precision [49,50].

The "stealthiness" parameter $\chi$ [28], given by

$$\chi = \frac{M(K)}{d(N-1)}, \tag{4}$$

is a measure of the relative fraction of constrained degrees of freedom compared to the total number of configurational freedoms available to the system, $d(N-1)$. In Eq. (4), $M(K)$ is the number of independently constrained wave vectors. In the the thermodynamic limit, the stealthiness parameter takes the form

$$\chi = \frac{v_1(K)}{\rho 2d(2\pi)^d}, \tag{5}$$

where $v_1(K)$ is the volume of a hypersphere of radius $K$ and $\rho$ is the number density. For $d \geqslant 2$ the dimensionality per particle of the configuration space, $d_C = d(1-2\chi)$, is expressed succinctly in terms of this parameter [28]. Ground states are disordered for $\chi < 1/2$ and crystalline otherwise in dimensions $d \geqslant 2$ [28,47,48,51] ($d = 1$ is a special case, discussed at length in Ref. [52]). There are infinite ways of sampling configurations from the ground-state manifold, each with its own probability measure [28].

Trajectories beginning from different initial conditions illuminate the nature of the energy landscape, which depends on $\chi$ and determines what portions of the ground-state manifold are sampled [28]. Targeting different portions of the ground-state manifold may allow one to design the functional form of the structure factor $S(k)$ of stealthy ground states at wave numbers outside of the exclusion region ($k > K$) and investigate how short- up to intermediate-wavelength density fluctuations vary across the manifold. Two types of initial conditions have been extensively used to attain disordered stealthy hyperuniform ground states: random (Poisson) configurations [26–28,43,44,46–50,53] and low-temperature equilibrated states [28,47]. The latter has been employed to generate entropically favored ground states. Much less is known about the relationship between other types of initial conditions and the final ground states. Interestingly, it is known that only very tiny collective, almost imperceptible, displacements of the particles initially arranged in the correlated but nonhyperuniform random sequential packing [54] are required to achieve stealthy hyperuniform ground states [2]. While this is an intriguing outcome, a systematic investigation of how the structural characteristics of the initial conditions biases what parts of the infinitely degenerate ground-state manifold are accessed has been largely lacking.

The purpose of this paper is to begin to address this problem by characterizing the trajectories of a variety of different two-dimensional (2D) initial configurations as a function of the computational time during the optimization until the ground states within the disordered regime ($0 < \chi < 1/2$) are reached. Specifically, we study initial conditions which span an array of antihyperuniform, nonhyperuniform, and hyperuniform systems with varying degrees of order and disorder across length scales evolved by collective-coordinate optimization. The initial conditions include configurations derived from a random sequential addition (RSA) process, those with Gaussian pair statistics (GAU), uniformly randomized

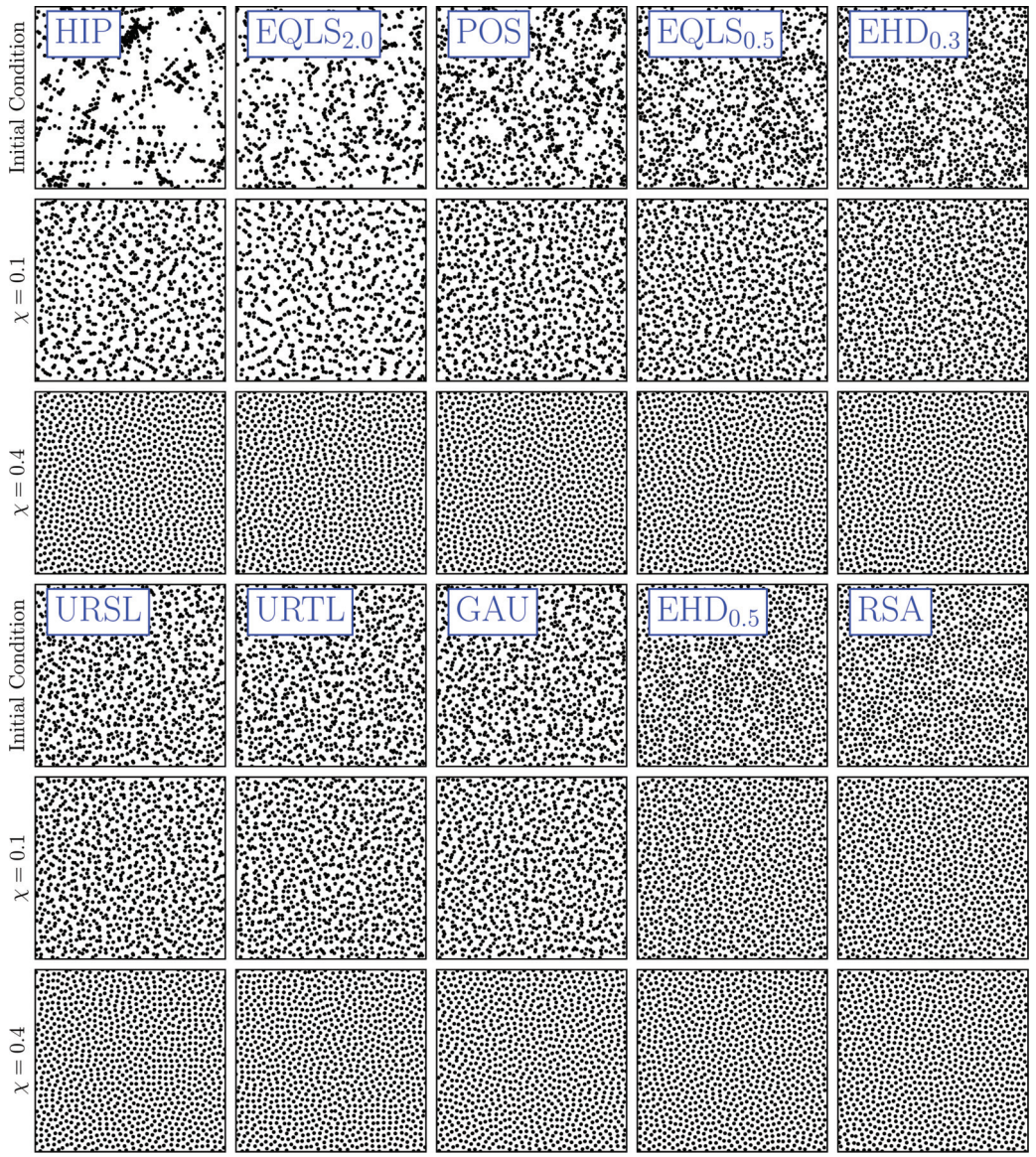



FIG. 1. Representative two-dimensional initial point patterns summarized in Table I and corresponding $\chi = 0.1$ and $\chi = 0.4$ stealthy ground states evolved from collective-coordinate optimization. From the top left to bottom right, structural differences between initial conditions and their associated ground states become increasingly difficult to detect visually. Similarly, stealthy ground states evolved from different initial conditions become increasingly difficult to distinguish with increasing $\chi$. We quantify these differences using the translational order metrics and proximity metric defined in Sec. II.

lattices [UR(S/T)L], ensembles of equilibrium hard disks at different volume fractions (EHD), a Poisson point process (POS), equiluminous point patterns (EQLS), and a hyperplane intersection process (HIP), all of which are listed in Table I, illustrated in Fig. 1, and defined precisely in Sec. III.

We characterize the trajectories from different initial conditions by computing a proximity metric $p_{t'}(t)$, translational order metric $\tau(t)$, and normalized local number variance $\sigma^2(t;R)/R^2$ as functions of the computational time $t$ until the associated ground state is reached for selected values of $\chi$. The time-dependent configurational proximity metric $p_{t'}(t)$, defined precisely in Sec. II, is used to quantify the distance between two different particle configurations, enabling one to analyze the degree of structural rearrangement required of different initial conditions to reach the ground-state manifold [53]. The translational order metric $\tau(t)$, also defined in Sec. II, is a sensitive measure of the degree of translation order in many-particle systems. The normalized local number variance $\sigma^2(t;R)/R^2$, defined in Sec. II A, quantifies local number density fluctuations and is intimately related to $S(k)$ of a point configuration [1].

We find that initial conditions with a greater degree of infinite- down to intermediate-wavelength density fluctuations are a larger configurational distance away from and take greater computational time to reach the ground-state manifold. Using the time-dependent proximity metric, we show that trajectories from hyperuniform states approach the ground-state manifold at the fastest rate among the initial conditions we consider, while trajectories from antihyperuniform states approach it at the slowest rate. The time-dependent

translational order metric highlights how initial conditions with suppressed infinite- down to intermediate-wavelength density fluctuations require a smaller computational time to reach a ground state. Separately, the normalized local number variance of stealthy ground states reflects distinct pair statistics in ground-state ensembles sampled by different initial conditions and highlights the effect of higher-order correlations on trajectories. Learning how to manipulate initial conditions in the optimization procedure to target different portions of the stealthy ground-state manifold enables one to explore structurally unique configurations along the manifold with designed short- up to intermediate-ranged spatial correlations (i.e., wave numbers $k > K$ outside the constrained exclusion region) for the purposes of materials discovery.

The paper is organized as follows: In Sec. II we provide basic definitions of the pair statistics, translational order metric, and proximity metric that are used to analyze point patterns. We define hyperuniform point processes and briefly summarize the numerical collective-coordinate optimization procedure for generating stealthy hyperuniform ground states. In Sec. III we expand on the initial conditions listed in Table I and describe their characteristic spatial correlations and algorithms to generate each configuration. The simulation procedure and algorithm we employ to minimize the potential (1) during collective-coordinate optimization is detailed in Sec. IV. The structure factor, translational order metrics, proximity metric, and local number variance of stealthy hyperuniform ground states evolved from different initial conditions at various $\chi < 1/2$ are reported in Sec. V.

## II. DEFINITIONS AND PRELIMINARIES

A point process in $d$-dimensional Euclidean space $\mathbb{R}^d$ is a distribution of an infinite number of points in $\mathbb{R}^d$ with the configuration $\boldsymbol{r}^N \equiv \boldsymbol{r}_1, \ldots, \boldsymbol{r}_N$ at a well-defined number density (number of points per unit volume). For a statistically homogeneous point process in $\mathbb{R}^d$ at number density $\rho$, the quantity $\rho^n g_n(\boldsymbol{r}^n)$ is the probability density associated with simultaneously finding $n$ points at locations $\boldsymbol{r}^n \equiv \boldsymbol{r}_1, \ldots, \boldsymbol{r}_n$ in $\mathbb{R}^d$ [55]. With this convention, each $n$-particle correlation function $g_n$ approaches unity when all of the points becomes widely separated from one another. Statistical homogeneity implies $g_n$ is translationally invariant and hence depends only on the relative displacement of the positions with respect to any chosen system origin, e.g., $g_n = g_n(\boldsymbol{r}_{12}, \ldots, \boldsymbol{r}_{1n})$ where $\boldsymbol{r}_{ij} = \boldsymbol{r}_j - \boldsymbol{r}_i$.

The pair correlation function $g_2(\boldsymbol{r})$ is a particularly important quantity. If a point process is also rotationally invariant (statistically isotropic), then $g_2$ depends on the radial distance $r \equiv |\boldsymbol{r}|$ only, i.e., $g_2(\boldsymbol{r}) = g_2(r)$. The total correlation function $h(\boldsymbol{r})$ is trivially related to $g_2(\boldsymbol{r})$ as follows [55]:

$$h(\boldsymbol{r}) \equiv g_2(\boldsymbol{r}) - 1. \tag{6}$$

When there are no long-range correlations in the system, $h(\boldsymbol{r}) \to 0$ or, equivalently, $g_2(\boldsymbol{r}) \to 1$ as $|\boldsymbol{r}| \to \infty$. The structure factor $S(\boldsymbol{k})$, which plays a prominent role in this paper, is related to the Fourier transform of $h(\boldsymbol{r})$, denoted by $\tilde{h}(\boldsymbol{k})$, via the expression [55]

$$S(\boldsymbol{k}) \equiv 1 + \rho\tilde{h}(\boldsymbol{k}). \tag{7}$$

A useful scalar positive order metric that captures the degree of translational order is the $\tau$ order metric [28] defined as

$$\begin{aligned}\tau &\equiv \frac{1}{D^d}\int_{\mathbb{R}^d}[g_2(\boldsymbol{r})-1]^2 d\boldsymbol{r} \\ &= \frac{1}{(2\pi D)^d\rho^2}\int_{\mathbb{R}^d}[S(\boldsymbol{k})-1]^2 d\boldsymbol{k},\end{aligned} \tag{8}$$

where $D$ is a characteristic microscopic length scale. In this paper, we take $D = \rho^{-1/2}$, which is a rough measure of the average separation between pairs of points. The $\tau$ order metric measures deviations of two-particle statistics from that of the Poisson distribution for which $\tau = 0$. Note that because both positive and negative correlations contribute to the integral, since the deviations of either $g_2(\mathbf{r})$ or $S(\boldsymbol{k})$ from unity are squared, this generally positive metric measures the degree of translational order across length scales. The $\tau$ order metric is closely related to the two-particle excess entropy [56], which accounts for a large proportion of the total configurational entropy of a point pattern. For the purpose of analyzing time-dependent trajectories, we study the time-dependent order metric $\tau(t)$ which corresponds to an integral over the time-dependent structure factor, $S(\boldsymbol{k};t)$.

For our analysis of the evolution to stealthy ground states, we also consider the decomposition of the $\tau(t)$ order metric within and beyond the exclusion radius $K$ separately:

$$\tau_{k\leqslant K}(t) = \frac{1}{(2\pi D)^d\rho^2}\int_0^K [S(\boldsymbol{k};t)-1]^2 d\boldsymbol{k}, \tag{9a}$$

$$\tau_{k>K}(t) = \frac{1}{(2\pi D)^d\rho^2}\int_K^\infty [S(\boldsymbol{k};t)-1]^2 d\boldsymbol{k}. \tag{9b}$$

The quantity $\tau_{k\leqslant K}(\infty)$ will converge to the same value for all initial conditions definition. By contrast, $\tau_{k>K}(\infty)$ will vary depending on both $\chi$ and the initial conditions from which it evolves.

The time-dependent configurational proximity metric $p_{t'}(t)$ is defined [53]

$$p_{t'}(t) \equiv \rho^{1/2}\left(\sum_{j=1}^N |\boldsymbol{r}_j(t) - \boldsymbol{r}_j(t')|^2\right)^{1/2}, \tag{10}$$

where $\boldsymbol{r}_j(t)$ is the position of the $j$th particle of the configuration at time $t$ during collective-coordinate optimization. We use $\rho^{-1/2}$ as a characteristic length scale of the system. The value of $p_{t'}(t)$ quantifies the distance of a time-evolving point pattern at time $t$ to a reference state from the same trajectory at time $t'$. This metric is applied *a posteriori* and requires the complete trajectory of an initial condition brought to a stealthy ground state. The *configurational distance from the ground-state manifold* is defined to be the difference between the total proximity metric and the proximity metric with reference to the initial condition, denoted $p_0(\infty) - p_0(t)$.

### A. Hyperuniform point processes

Consider uniformly sampling the number of points that are contained within a spherical window of radius $R$ of a point process in $\mathbb{R}^d$. A hyperuniform point process has the property that the local number variance $\sigma^2(R) \equiv \langle N(R)^2\rangle - \langle N(R)\rangle^2$ grows more slowly than $R^d$ [1]. Because $\sigma^2(R)$ is exactly

related to a $d$-dimensional volume integral of the structure factor $S(\boldsymbol{k})$, this implies that hyperuniform states of matter posses infinite wavelength density fluctuations (appropriately normalized) that vanish, i.e., $S(\boldsymbol{k})$ obeys the condition

$$\lim_{|\boldsymbol{k}|\to 0} S(\boldsymbol{k}) \to 0, \tag{11}$$

which means they are poised at an "inverted" critical point with associated scaling exponents [1]. For a Poisson (spatially uncorrelated) point process, including typical liquids and structural glasses, the number variance grows like the volume of the window, i.e., $\sigma^2(R) \sim R^d$, implying that $S(\boldsymbol{k})$ is positive at $\boldsymbol{k} = \boldsymbol{0}$. All *perfect* crystals and quasicrystals are hyperuniform such that $\sigma^2(R) \sim R^{d-1}$; in other words, the number variance grows like the window surface area [1]. In recent years, evidence has been emerging that disordered hyperuniform many-particle systems can be regarded as new distinguishable states of disordered matter (see examples from Torquato [2] and references therein).

Whenever the structure factor goes to zero with the power law form $S(\boldsymbol{k}) \sim |\boldsymbol{k}|^{\alpha}$, the number variance has the following large-$R$ asymptotic scaling that depends on the value of the exponent $\alpha$ [57,58]:

$$\sigma^2(R) \sim \begin{cases} R^{d-1}, & \alpha > 1 \quad \text{(Class I)} \\ R^{d-1}\ln R, & \alpha = 1 \quad \text{(Class II)} \\ R^{d-\alpha}, & 0 < \alpha < 1 \quad \text{(Class III).} \end{cases} \tag{12}$$

Since disordered as well as ordered stealthy states can be viewed as systems in which $\alpha$ tends to infinity [28], we see from Eq. (12) that they have the asymptotic scaling $\sigma^2(R) \sim R^{d-1}$.

By contrast, for any nonhyperuniform system, the local number variance has the following large-$R$ scaling behaviors [59]:

$$\sigma^2(R) \sim \begin{cases} R^d, & \alpha = 0 \quad \text{(typical nonhyperuniform)} \\ R^{d-\alpha}, & -d < \alpha < 0 \quad \text{(antihyperuniform).} \end{cases} \tag{13}$$

For a "typical" nonhyperuniform system, $S(0)$ is bounded [2]. In antihyperuniform systems, $S(0)$ is unbounded, i.e.,

$$\lim_{k\to 0} S(k) \to +\infty, \tag{14}$$

and hence are diametrically opposed to hyperuniform systems [59]. Antihyperuniform systems include fractals, systems at thermal critical points [60–64], as well as certain substitution tilings [65].

### B. Collective-coordinate optimization

As detailed in the Introduction, we simulate point processes in periodic fundamental cells with the total potential given by a sum of pairwise potentials as in Eq. (1). The total potential can be simplified as

$$\Phi^*(\boldsymbol{r}^N) = \Phi(\boldsymbol{r}^N) - \Phi_0 = \frac{N}{2V_\Omega}\sum_{k\leqslant K} \tilde{v}(\boldsymbol{k})S(\boldsymbol{k}), \tag{15}$$

with $\Phi_0 = -Nv(\boldsymbol{0})/2V_\Omega$ the structure-independent contribution to the total energy that depends on $\tilde{v}(\boldsymbol{k})$ [28]. The global minimum of $\Phi^*(\boldsymbol{r}^N)$ is zero, and convergence is achieved below an arbitrary tolerance that we make $\Phi^* < 10^{-22}$. The family of "stealthy" pair potentials are defined [26,27,44,46,52,53],

$$\tilde{v}(\boldsymbol{k}) = \begin{cases} V(k) & \text{if} \quad k \leqslant K, \\ 0 & \text{otherwise,} \end{cases} \tag{16}$$

where $V(k)$ is a positive isotropic function and $K$ is the radius of the exclusion region. In this paper we always take $V(k) = 1$. Taking the gradient of (15) yields the force on particles:

$$\boldsymbol{F}_j = -\nabla_j \Phi^*(\boldsymbol{r}^N) = \frac{1}{V_\Omega}\sum_{k\leqslant K} \boldsymbol{k}\tilde{v}(\boldsymbol{k})\mathrm{Im}[\tilde{n}(\boldsymbol{k})\exp(i\boldsymbol{k}\cdot\boldsymbol{r}_j)]. \tag{17}$$

This relation enables us to perform energy minimizations which we do using Newton's method,

$$\boldsymbol{r}^N_{m+1} = \boldsymbol{r}^N_m - \gamma\nabla\Phi^*\left(\boldsymbol{r}^N_m\right). \tag{18}$$

The dimensionless step size $\gamma\rho^{1/2}$ is related to the time step as $\Delta t = \gamma\rho^{1/2}$ at each iteration $m$ of the algorithm. The total computational time $T = \sum_j \Delta t_j$ required for a trajectory to reach a stealthy ground state (defined to be when $\Phi^* < 10^{-22}$; see Sec. II B below) will be used to make time dimensionless. Numerical evidence [44] has shown that for $\chi < 1/2$ the stealthy energy landscape is devoid of local minima and the ground-state manifold is the only outcome for gradient descent trajectories. The ground states we study are limited to $\chi < 1/2$, and, indeed, our optimization procedure only ever converges to a disordered stealthy ground state.

## III. INITIAL CONDITIONS

### A. Hyperplane intersection processes

The hyperplane intersection process (HIP) is a point process originating from a tessellation formed by a collection of intersecting randomly oriented and uniformly distributed hyperplanes in Euclidean space [66]. Since hyperplanes span the entire space, infinitely long-ranged correlations are induced between points and arbitrarily large density fluctuations persist as the system size grows arbitrarily large [2]. Consequently, $S(k)$ diverges as $k \to 0$, and these configurations are antihyperuniform [59]. Point patterns derived from the hyperplane intersection process are generated using the simulation procedure described in the supporting information provided by Klatt *et al.* [67].

### B. Equiluminous point patterns

An equiluminous point pattern with luminosity $I$ (EQLS$_I$) is one in which the structure factor is a constant $I$ for a range of wave vectors [27]. The equiluminous point patterns we consider have $S(k) = 0.5$ and $S(k) = 2$ for $0 < k \leqslant Q$ and are unconstrained otherwise, where $Q$ is the radius of the exclusion region of the stealthy ground states with the largest $\chi$ we consider, corresponding to $\chi = 0.45$. We use these configurations as initial conditions because they are nonhyperuniform with strong clustering due to constraints applied to the structure factor. Equiluminous configurations are generated using the collective-coordinate optimization procedure while targeting a nonzero $S(k)$ within the exclusion region.

### C. Poisson point patterns

The simplest initial condition we consider is a statistically homogeneous and isotropic Poisson point process (POS) at number density $\rho$. We use these point patterns as initial conditions because they are spatially uncorrelated across all of space and, since $S(k) = 1$ for all $k$, are therefore nonhyperuniform. Configurations derived from a Poisson point process are generated by uniformly distributing points at number density $\rho = 1$ within the simulation box without regard for other particles or overlaps.

### D. Uniformly randomized lattices

Uniformly randomized lattices (URLs) are perturbed lattices that uniformly randomly displace each lattice point in a rescaled unit cell of the lattice $bC = \{\boldsymbol{x} \in \mathbb{R}^d : \boldsymbol{x}/b \in C\}$, with $C$ the unit cell and $b > 0$ a scalar controlling the strength of the perturbation [68,69]. The scattering intensity of a URL configuration contains a diffuse contribution and typically inherits the Bragg peaks (long-ranged order) of the progenitor lattice while preserving hyperuniformity: the angular-averaged structure factor behaves like $S(k) \sim k^2$ as $k \to 0$ [70]. As such, they are class I hyperuniform. Klatt *et al.* showed that when $b$ takes on integer values all Bragg peaks of the URL vanish and the resultant configuration is "cloaked" in the sense that the progenitor lattice cannot be reconstructed from pair statistics alone [69]. In what follows we consider only cloaked URL initial conditions. We use different URL configurations as initial conditions because they are hyperuniform and inherit periodicity in certain higher-order correlation functions from their progenitor lattices [69]. In this paper we study two kinds of uniformly randomized lattice, one derived from the square lattice $\mathbb{Z}^2$ (URSL) and another derived from the triangular lattice (URTL), each with rescaled unit cells of strength $b = 1$ centered at the lattice points. The rescaled unit cell of $\mathbb{Z}^2$ is a square of side length $b$. The rescaled unit cell of the hexagonal lattice is a rhombus of side length $b$ and acute angle $\pi/3$.

### E. Gaussian pair statistics

As another initial condition, we consider a class I hyperuniform system in which the total correlation function is the following Gaussian:

$$h(r) = -\exp\left(-\pi\rho r^2\right), \tag{19}$$

with a corresponding structure factor given by

$$S(k) = 1 - \exp\left(-k^2/4\pi\rho\right). \tag{20}$$

Point patterns with Gaussian pair statistics (GAU) are generated using the inverse algorithm described by Wang and Torquato [71]. In what follows we set the number density of these configurations to $\rho = 1$. Such pair statistics are exactly achieved by the one-component plasma at a special value of the coupling constant [72]. We employ these systems as initial conditions because they are hyperuniform and can be generated without reference to a progenitor lattice, unlike the URL systems. This model represents the low-density, high-temperature limit of $S(k)$ for the Gaussian-core model, known to exhibit anomalous phase behaviors such as negative thermal expansion and reentrant melting [73,74]. Gaussian pair statistics incorporate soft-core short-ranged repulsions found in macromolecules and are commonly used to model polymer systems [75,76].

### F. Equilibrium hard disks

We consider identical hard disks of radius $a$ at a volume fraction $\phi$ in equilibrium ($\text{EHD}_\phi$) [54]. We use this initial condition because it is nonhyperuniform with significant short-ranged spatial correlations. Long-ranged spatial correlations become significant only at sufficiently large volume fractions [54]. This model exhibits rich phase behavior and effectively approximates the structure of dense particle systems with more complicated potentials [55]. Ensembles of equilibrium hard disks are generated using Monte Carlo methods [54] at two different volume fractions, $\phi = 0.3$ and $\phi = 0.5$, given by $\phi = \rho v_1(a)$ in terms of the number density $\rho$ and area of the circle of radius $a$, $v_1(a)$.

### G. Saturated random sequential adsorption

Random sequential adsorption (RSA) is a time-dependent process that irreversibly, randomly, and sequentially places nonoverlapping particles into a prescribed volume [54,77,78]. In the infinite-time limit, the system becomes saturated at a volume fraction $\phi \approx 0.5470735$ [78,79]. Point patterns derived from RSA processes are nonhyperuniform, though the hard core constraint induces a significant degree of short-ranged order in these configurations: In the thermodynamic limit, the structure factor at the origin is $S(0) \approx 0.05$ [80]. We use this initial condition because it is nearly hyperuniform. An ensemble of initial conditions derived from the centroids of disks in 2D saturated RSA packings was generated using the algorithm detailed by Zhang and Torquato [79].

## IV. SIMULATION PROCEDURE

Generating disordered stealthy hyperuniform systems involves finding true ground states of $\Phi$ in Eq. (1). The pair potential (16) we use is

$$\tilde{v}(k) = \begin{cases} V_0 & \text{if} \quad k \leqslant K, \\ 0 & \text{if} \quad k > K, \end{cases} \tag{21}$$

with $V_0 = 1$. To minimize the potential we employ a derivative-based algorithm. The first term on the rightmost side of (15) is provided to the algorithm as the objective function and the negative of the force in (17) is provided as the gradient. In order to minimize energy we employ a local gradient descent algorithm with the following steps [47]:

a. Start from an initial point pattern $\boldsymbol{x}$ and evaluate the objective function $\Phi^*(\boldsymbol{x})$ and associated gradient $\nabla\Phi^*$.

b. Beginning from a relatively large step size $\gamma\rho^{1/2} = 10^{-3}$, calculate the vector $\Delta\boldsymbol{x} = -\gamma\nabla\Phi^*/|\nabla\Phi^*|$. Find the function value at the next step $\Phi^*(\boldsymbol{x} + \Delta\boldsymbol{x})$. Calculate the change of function value $\Delta\Phi^* = \Phi^*(\boldsymbol{x} + \Delta\boldsymbol{x}) - \Phi^*(\boldsymbol{x})$.

c. When a downhill step is successful the step size $\gamma$ is increased by a factor of two. Otherwise, the algorithm backtracks and the step size is decreased by a factor of two.

d. Repeat the above steps until a minimum is found with enough precision.

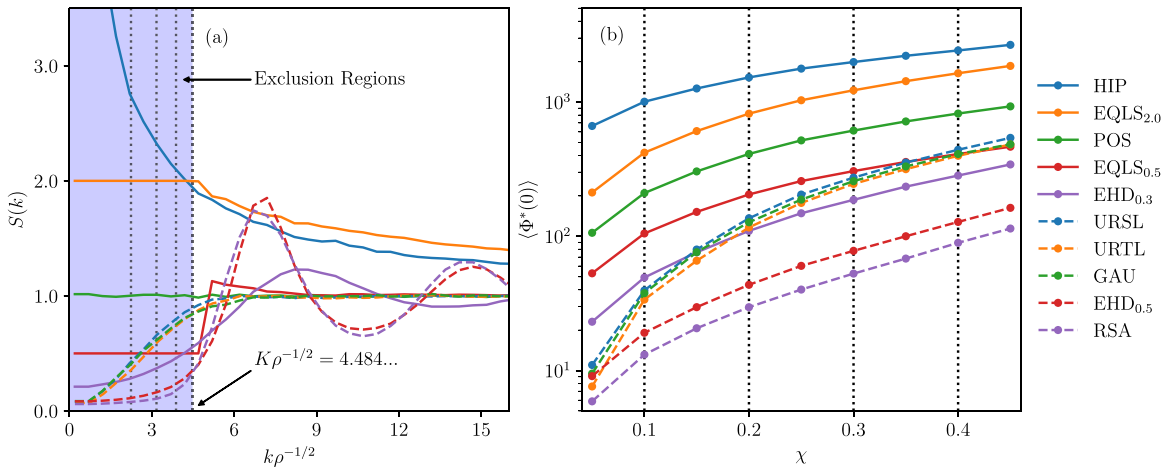



FIG. 2. Characteristics of the initial conditions summarized in Table I. (a) Structure factor $S(k)$ versus dimensionless wave number $k\rho^{-1/2}$ for each initial condition. Shaded in blue is the exclusion region corresponding to the $\chi = 0.4$ ground-state manifold and dotted lines correspond to dimensionless wave numbers $k\rho^{-1/2} = 2.242...$, $3.171...$, $3.883...$, and $4.484...$. (b) Potential energy of each initial condition for various $0.05 \leqslant \chi \leqslant 0.45$. Dotted lines coincide with values of $\chi$ corresponding to exclusion radii at the dimensionless wave numbers indicated in (a).

For $\chi < 1/2$ the objective function always ends up being very close to zero (the minimum) [47]. The maximum ending objective function for this algorithm is as high as $10^{-18}$ for the evolution of different initial conditions to a $\chi = 0.45$ stealthy ground state. For the evolution to ground states with $\chi < 0.45$, the final objective function does not exceed $10^{-20}$. We find that the temporal dependence of trajectories evolved from different initial conditions to stealthy ground states with $\chi < 0.5$ are insensitive to the energy tolerance for $\Phi^* < 10^{-10}$. With this scheme, simulations to record trajectories take no longer than 24 hours on an Intel CPU for the largest $\chi$ we consider. Computing the time-dependent structure factor and local number variance for these trajectories takes around 6 hours on an NVIDIA A100 GPU.

## V. RESULTS AND DISCUSSION

In this section we present the analysis of trajectories to stealthy ground states evolved from the initial conditions summarized in Table I for with $0.05 \leqslant \chi \leqslant 0.45$. Representative configurations from the $\chi = 0.1$ and $\chi = 0.4$ ground-state ensembles sampled by each initial condition are shown in Fig. 1. In the Supplemental Material [81], we provide a movie that shows the evolution of HIP, POS, and GAU initial conditions to their respective stealthy ground states with $\chi = 0.4$. The structure factors of each initial condition as well as the exclusion regions for certain values of $\chi$ are illustrated in Fig. 2. The time-dependent proximity metric, translational order metric, and local number variance, all defined in Sec. II, are used to study trajectories to the stealthy ground-state manifold.

### A. Potential energy of initial conditions

Figure 2 demonstrates that density fluctuations contained only within the exclusion region (infinite down to intermediate wavelengths), where the structure factor $S(k)$ must be zero in the ground state, contribute to the potential energy of an initial condition. For fixed $\chi$, the potential $\langle\Phi^*(0)\rangle$ increases as the area under $S(k)$ for $k \leqslant K$ of an initial condition increases, seen by comparing Figs. 2(a) and 2(b). Figure 2(b) shows that the ensemble-averaged energy of the initial condition $\langle\Phi^*(0)\rangle$ increases as $\chi$ increases for all initial conditions due to the exclusion radius $K$ increasing with $\chi$ to include a greater number of wave vectors in the summation of Eq. (1). Since $S(k)$ must be zero in the exclusion region, it is reasonable to expect that initial conditions with larger $\langle\Phi^*(0)\rangle$ will take a longer computational time to reach the ground-state manifold. Since $S(k)$ is unconstrained for wave numbers outside the exclusion region, density fluctuations at wave numbers $k > K$ in the initial conditions of Fig. 2(a) will influence $S(k)$ for $k > K$ in stealthy ground states and enable one to design the short- and intermediate-wavelength density fluctuations of stealthy configurations. Intersections between curves of $\langle\Phi^*(0)\rangle$ versus $\chi$ in Fig. 2(b) reflect differences in the infinite- down to intermediate-wavelength scaling of $S(k)$ versus $k\rho^{-1/2}$ across the different initial conditions we consider. The relative increase in $\langle\Phi^*(0)\rangle$ between the $\chi = 0.05$ and 0.45 ground-state manifolds is largest for the hyperuniform initial conditions (URSL, URTL, and GAU), due to their small-$k$ behavior $S(k) \sim k^2$, while it is smallest for the antihyperuniform HIP, since $S(k)$ diverges as $k \to 0$ and decreases as $k$ increases. In Sec. V B we quantify the relationship between the energy of an initial condition and its configurational distance from the ground-state manifold.

### B. Time-dependent configurational distance from a stealthy ground state

Figure 3 highlights how initial conditions with a larger potential energy are a larger configurational distance from the ground-state manifold. Figures 3(a) and 3(b) show at $t = 0$, both $p_0(\infty) - p_0(t)$ and $\Phi^*(t)$ increase as the degree of intermediate- and long-range disorder of an initial condition increases for trajectories to the $\chi = 0.4$ ground-state manifold. We note that this result is true in general for $\chi < 0.5$ even though it is $\chi$-dependent. The effect of infinite- down to

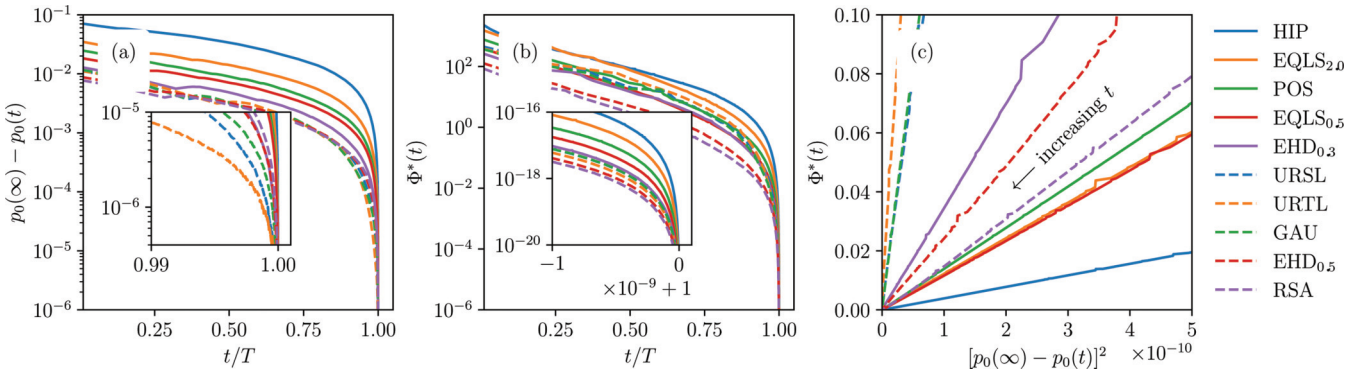



FIG. 3. Plots of the time-dependent configurational distance from a stealthy ground state $p_0(\infty) - p_0(t)$ and the potential energy $\Phi^*(t)$ versus the dimensionless computational time $t/T$ of trajectories from various initial conditions to $\chi = 0.4$ stealthy ground states, where $T$ is the total computational time defined in Sec. II. (a) The distance $p_0(\infty) - p_0(t)$ as a function of $t/T$. (b) The potential $\Phi^*(t)$ as a function of $t/T$. (c) The potential $\Phi^*(t)$ versus $[p_0(\infty) - p_0(t)]^2$, both parameterized by $t$, for trajectories to stealthy ground states that are a small distance away from the manifold. Qualitative trends observed in this plot, including the rates at which each initial condition approach the ground-state manifold, are true of trajectories to ground states for all $\chi < 0.5$ we investigate.

intermediate-wavelength density fluctuations on $p_0(\infty)$ and $\Phi^*(0)$ is reflected in Fig. 2(a) and indicates that the computational time required to reach a ground state increases as the potential energy increases. As $t/T$ increases in Figs. 2(a) and 2(b), with $T$ the total computational time of the trajectory defined in Sec. II, both $p_0(\infty) - p_0(t) = 0$ and $\Phi^*(t) = 0$ and correspond to when the trajectory has reached a ground state. At large $t/T$, both $p_0(\infty) - p_0(t)$ and $\Phi^*(t)$ sharply decrease for all initial conditions and signal that topography of the energy landscape close to the ground-state manifold is much steeper than it is farther away from the manifold. Intersections between curves in both plots indicate that trajectories approach the ground-state manifold at different rates, highlighted by the insets of Figs. 3(a) and 3(b). We specifically observe in these plots that at large $t/T$, $p_0(\infty) - p_0(t)$ and $\Phi^*(t)$ decrease the fastest for the hyperuniform initial conditions (URSL, URTL, and GAU), a result of preexisting infinite-wavelength structural order in these point patterns. Figure 3(c) shows that at small distances from the ground-state manifold $\Phi^*(t)$ scales quadratically with $p_0(\infty) - p_0(t)$ and is fastest for the hyperuniform initial conditions (URSL, URTL, and GAU) and slowest for the antihyperuniform initial condition (HIP). This result persists for trajectories evolved to stealthy ground states for all $0.05 \leqslant \chi \leqslant 0.45$ we consider, although the rate at which $\Phi^*(t)$ scales with $[p_0(\infty) - p_0(t)]^2$ for each initial condition differs for different $\chi$. This behavior suggests that topography of the energy landscape surrounding trajectories evolved from hyperuniform initial conditions is steepest while that surrounding trajectories evolved from antihyperuniform initial conditions is shallowest.

### C. Time-dependent translational order and number density fluctuations

Figure 4 demonstrates how the time-dependent translational order originating from the exclusion region and local number variance at large length scales quantitatively captures the differences between spatial correlations that characterize an initial condition and corresponding stealthy ground state. Figure 4(a) shows at $t/T = 0$, $\tau_{k\leqslant K}(t)$ increases as the strength of intermediate and long-ranged spatial correlation increases and corresponds to the extent to which $S(k)$ deviates from unity within the exclusion region for each initial condition in Fig. 2(a). The deviation of $\tau_{k\leqslant K}(t)$ from a straight line between $t/T = 0$ and $t/T = 1$ increases as $p_0(\infty)$ increases in Fig. 3(a), reflecting how initial conditions with spatial correlations similar to those of a stealthy configuration are a smaller configurational distance away from the ground-state manifold. Between $t = 0$ and $t = T$, $\tau_{k\leqslant K}(t)$ corresponding to EQLS$_{2.0}$ initially decreases because positive spatial correlations due to clustering in the initial condition are reduced,

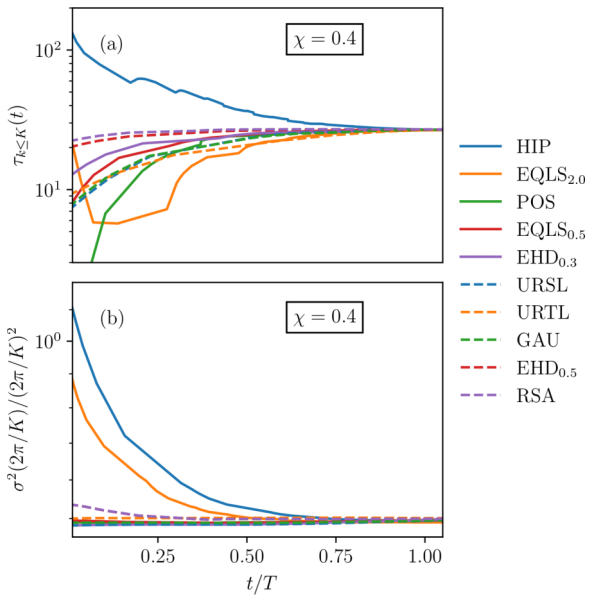



FIG. 4. Time-dependent translational order metric $\tau_{k\leqslant K}(t)$ and normalized local number variance $\sigma^2(t; R_0)/R_0^2$ for trajectories from each initial condition evolved to the $\chi = 0.4$ ground-state manifold. (a) Time-dependent translational order originating from the exclusion region $\tau_{k\leqslant K}(t)$ versus the dimensionless time $t/T$. (b) Local number variance evaluated at $2\pi/K \approx 1.4$ versus the dimensionless time $t/T$.

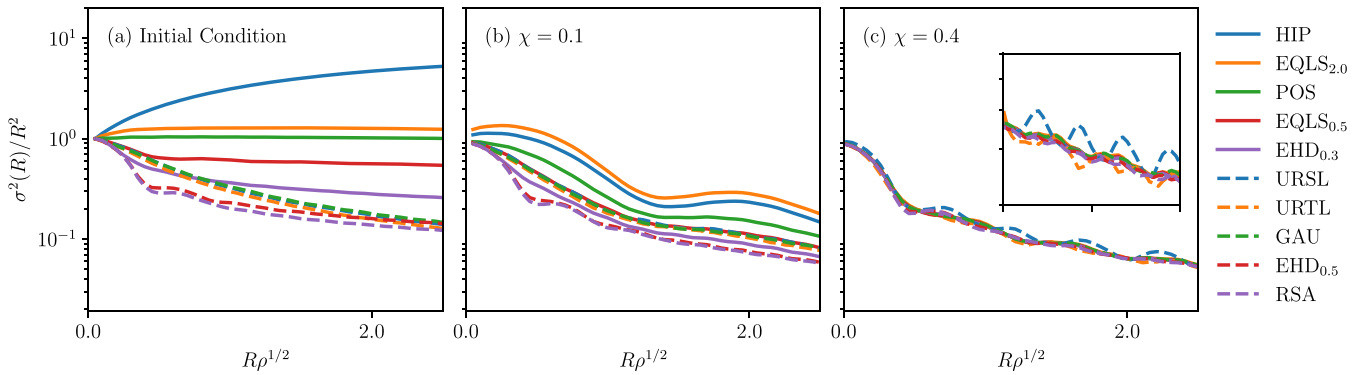



FIG. 5. Semilog plots of the normalized local number variance $\sigma^2(R)/R^2$ versus the dimensionless distance $R\rho^{1/2}$ in (a) each initial condition and their corresponding (b) $\chi = 0.1$ and (c) $\chi = 0.4$ stealthy ground states. Oscillations in $\sigma^2(R)/R^2$ in ground states with $\chi = 0.4$ evolved from the URL configurations in (c) indicate long-ranged order.

while at later times it increases because negative spatial correlations emerge as the stealthy ground state is approached. The values of $\tau_{k\leqslant K}(t)$ at $t = 0$ and $t = T$ for this initial condition are identical because this metric does not discriminate between positive and negative spatial correlations between pairs of points. The value of $\tau_{k\leqslant K}(t)$ at $t/T = 1$ is the same in stealthy configurations evolved from different initial conditions, since $S(k)$ of ground states are identical for $k \leqslant K$. Figure 4(b) shows $\sigma^2(t;R_0)/R_0^2$ at $R_0 \equiv 2\pi/K$, chosen since it is a characteristic length scale of stealthy ground states independent of the initial condition, decreases monotonically with the dimensionless time $t/T$, reflecting the emergence of long-ranged order as a trajectory approaches a ground state. The value of $\sigma^2(t;R_0)/R_0^2$ at $t/T = 0$ increases as the degree of intermediate- and long-ranged disorder of an initial condition increases, while when $t/T = 1$, it achieves a value that depends on $K$. As a consequence of their dependence on $K$, the values of $\tau_{k\leqslant K}(t)$ and $\sigma^2(t;R_0)/R_0^2$ at $t/T = 1$ will depend on $\chi$ (the latter is reported for stealthy ground states with $\chi = 0.1$ and 0.4 in Sec. V D).

### D. Differences in ground-state ensembles sampled by different initial conditions

Figures 5 and 6 illustrate that stealthy ground states evolved from different initial conditions are distinguished by their number density fluctuations at intermediate- down to small-length scales. Comparing Figs. 5(a) and 5(b), one sees that the large-$R$ value of $\sigma^2(R)/R^2$ (at the right edge of the plots) rank-orders the degree of disorder in the initial conditions similarly to how it rank-orders that of their corresponding stealthy ground states. This is a reflection of the observation in Fig. 3 that initial conditions with a small potential energy $\langle\Phi^*(0)\rangle$ are a small configurational distance away from the ground-state manifold. Figure 5(c) further demonstrates that when $\chi = 0.4$, the reduced dimensionality of the ground-state manifold causes $\sigma^2(R)/R^2$ in stealthy configurations evolved from different initial conditions to converge onto a single curve, except for those evolved from both URL configurations, which each oscillate at large-$R$, indicating long-ranged order [82]. Indeed, Fig. 6 shows $S(k)$ in ground states evolved from URL configurations have peaks that grow increasingly pronounced as $\chi$ increases and occur at values of $k\rho^{-1/2}$ which coincide exactly with those of the first Bragg peak in $S(k)$ of their corresponding progenitor lattices. Although the GAU and URL are in the same hyperuniformity class and share similar pair statistics across short-, intermediate-, and large-length scales, $S(k)$ in stealthy configurations evolved from the former are absent of sharp peaks. This contrast suggests trajectories to ground states are affected by correlation functions beyond the two-point level, since periodicity in the four-point correlation function of a URL is inherited from periodicity in the progenitor lattice [69].

## VI. CONCLUSIONS

Starting from a wide class of initial two-dimensional point configurations, we studied the evolution of trajectories of

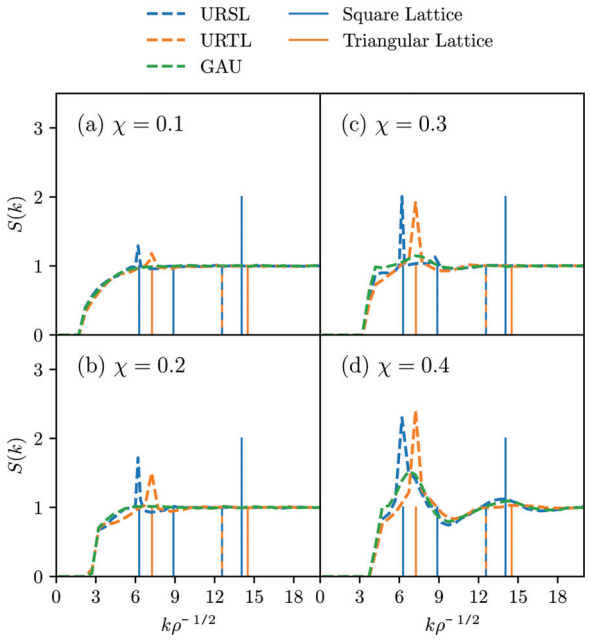



FIG. 6. Structure factor $S(k)$ versus the dimensionless wave number $k\rho^{-1/2}$ for stealthy ground states with $\chi = 0.1, 0.2, 0.3$, and 0.4 evolved from URSL, URTL, and GAU configurations as well as the first few Bragg peaks of the URL progenitor lattices. The dashed vertical line indicates a Bragg peak common to the square and triangular lattices.

the collective-coordinate optimization procedure to their corresponding disordered stealthy hyperuniform ground states as a function of $\chi$ in the disordered regime ($0 < \chi < 0.5$). We showed that the time-dependent proximity metric $p_0(t)$ illuminates how topography of the energy landscape far from the ground-state manifold is relatively shallow, compared to very close to the manifold where the landscape drops abruptly, and that infinite-wavelength density fluctuations characterizing an initial condition are reflected in the landscape topography. Trajectories from different initial conditions are distinguished by temporal evolution of the translational order metric $\tau_{k\leqslant K}(t)$ and the number density fluctuations $\sigma^2(t;R_0)/R_0^2$ at an intermediate length scale $R_0 \equiv 2\pi/K$. In conjunction with ground-state pair statistics from these trajectories, these metrics quantify how different initial conditions sample portions of the disordered ground-state manifold with unique structure factors for wave numbers outside of the stealthy exclusion region ($k > K$), i.e., from intermediate down to short wavelengths. The behavior of each of $p_0(t)$, $\tau_{k\leqslant K}(t)$, and $\sigma^2(t;R_0)/R_0^2$ reflects density fluctuations contained within the exclusion region characterizing an initial condition. As $S(k)$ increases for $k \leqslant K$, the difference between the values of both $p_0(t)$ and $\sigma^2(t;R_0)/R_0^2$ between $t = 0$ and $t = T$ increases and the deviation of $\tau_{k\leqslant K}(t)$ from a straight line along the same interval of time increases. In stealthy ground states with $\chi \geqslant 0.4$, although trajectories remain distinguishable, different initial conditions sample from ground-state ensembles with nearly identical number density fluctuations across short, intermediate, and large length scales, except for those evolved from the URL, which follow trajectories affected by spatial correlations beyond the two-point level.

Figure 7 presents a schematic of a projection of the stealthy energy landscape with $\chi < 0.5$, which is adapted from Ref. [43], but with added detail to reflect topography of the landscape surrounding trajectories evolved from different initial conditions. Dark lines represent the ground-state manifold running through the square lattice, denoted by a white square, and the triangular lattice, denoted by a white triangle. Dashed gray lines represent equipotential curves and indicate steepness of the energy landscape, information of which was not included in Ref. [43]. Each initial condition is represented with a white circle and its trajectory to a stealthy ground state with a blue arrow; straight red lines indicate the *displacement* of each initial condition from the portion of the ground-state manifold it samples and represent $p_0(\infty)$ and hence the evolution of both $\tau_{k\leqslant K}(t)$ and $\sigma^2(t;R_0)/R_0^2$ between the initial and ground-state configurations for each trajectory. The energy landscape is steepest in regions around the hyperuniform URSL due to the infinite-wavelength structural order that characterizes this configuration. The portion of the ground-state manifold sampled by the URSL is close to that which contains the square lattice, reflected in Fig. 6, and suggests that trajectories to a stealthy ground state are influenced by higher-order correlation functions beyond the two-point level [69]. By contrast, the energy landscape is shallowest in regions around trajectories from the antihyperuniform HIP because infinite-wavelength density fluctuations that characterize this initial configuration diverge. The hyperuniform, nonhyperuniform, and antihyperuniform initial

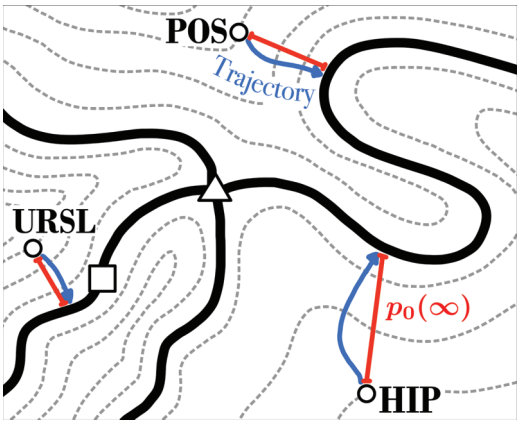



FIG. 7. Schematic of the stealthy energy landscape with $\chi < 0.5$ adapted from [43]. Dark lines represent the ground-state manifolds including the square lattice (white square) and triangular lattice (white triangle). Dashed gray lines are equipotential curves. White circles represent initial conditions, blue arrows represent their trajectories to a ground state, and straight red lines represent $p_0(\infty)$ and hence the evolution of both $\tau_{k\leqslant K}(t)$ and $\sigma^2(t;R_0)/R_0^2$ between the initial and ground-state configurations for each trajectory. The value of $p_0(\infty)$ is smallest when topography of the energy landscape surrounding a trajectory from the initial condition is steepest, represented by the trajectory evolved from the URSL, while it is largest when the landscape is most shallow, seen in trajectories evolved from the HIP.

conditions (not shown in this figure) occupy regions of the energy landscape near the URSL, POS, and HIP, respectively, and are a distance away from the ground-state manifold that increases as the area under $S(k)$ for $k \leqslant K$ increases in Fig. 2.

With unique structure factors beyond the exclusion region, stealthy ground states evolved from different initial conditions provide insight into the frequency with which structurally unique configurations occur along the ground-state manifold and, in turn, the nonuniform probability measure with which different initial conditions sample the manifold [28]. Manipulating the initial condition hence provides a route to the inverse design of stealthy hyperuniform media with tunable short- and intermediate-ranged spatial correlations for materials discovery [83].

## ACKNOWLEDGMENTS

S.J.D. thanks Jaeuk Kim, Murrak Skolnick, and Carlo Vanoni for their very helpful feedback on the manuscript. This work was supported by the Army Research Office under Cooperative Agreement No. W911NF-22-2-0103. The computational work reported in this paper was substantially performed used the Princeton Research Computing resources at Princeton University, which is a consortium of groups led by the Princeton Institute for Computational Science and Engineering (PICSciE) and Research Computing.

## DATA AVAILABILITY

The data that support the findings of this article are not publicly available. The data are available from the authors upon reasonable request.

[1] S. Torquato and F. H. Stillinger, Local density fluctuations, hyperuniform systems, and order metrics, Phys. Rev. E **68**, 041113 (2003).

[2] S. Torquato, Hyperuniform states of matter, Phys. Rep. **745**, 1 (2018).

[3] Y. Jiao, T. Lau, H. Hatzikirou, M. Meyer-Hermann, J. C. Corbo, and S. Torquato, Avian photoreceptor patterns represent a disordered hyperuniform solution to a multiscale packing problem, Phys. Rev. E **89**, 022721 (2014).

[4] A. Mayer, V. Balasubramanian, T. Mora, and A. M. Walczak, How a well-adapted immune system is organized, Proc. Natl. Acad. Sci. USA **112**, 5950 (2015).

[5] C. E. Zachary, Y. Jiao, and S. Torquato, Hyperuniform long-range correlations are a signature of disordered jammed hard-particle packings, Phys. Rev. Lett. **106**, 178001 (2011).

[6] Y. Jiao and S. Torquato, Maximally random jammed packings of Platonic solids: Hyperuniform long-range correlations and isostaticity, Phys. Rev. E **84**, 041309 (2011).

[7] P. Rissone, E. I. Corwin, and G. Parisi, Long-range anomalous decay of the correlation in jammed packings, Phys. Rev. Lett. **127**, 038001 (2021).

[8] C. E. Maher, Y. Jiao, and S. Torquato, Hyperuniformity of maximally random jammed packings of hyperspheres across spatial dimensions, Phys. Rev. E **108**, 064602 (2023).

[9] F. J. Dyson, Correlations between eigenvalues of a random matrix, Commun. Math. Phys. **19**, 235 (1970).

[10] S. Torquato, A. Scardicchio, and C. E. Zachary, Point processes in arbitrary dimension from Fermionic gases, random matrix theory, and number theory, J. Stat. Mech. (2008) P11019.

[11] H. Wang, R. Samajdar, and S. Torquato, Correlations in interacting electron liquids: Many-body statistics and hyperuniformity, Phys. Rev. B **110**, 104201 (2024).

[12] R. L. Jack, I. R. Thompson, and P. Sollich, Hyperuniformity and phase separation in biased ensembles of trajectories for diffusive systems, Phys. Rev. Lett. **114**, 060601 (2015).

[13] D. Hexner and D. Levine, Hyperuniformity of critical absorbing states, Phys. Rev. Lett. **114**, 110602 (2015).

[14] D. Hexner, P. M. Chaikin, and D. Levine, Enhanced hyperuniformity from random reorganization, Proc. Natl. Acad. Sci. USA **114**, 4294 (2017).

[15] S. Wilken, A. Chaderjian, and O. A. Saleh, Spatial Organization of Phase-Separated DNA Droplets, Phys. Rev. X **13**, 031014 (2023).

[16] K. J. Wiese, Hyperuniformity in the manna model, conserved directed percolation and depinning, Phys. Rev. Lett. **133**, 067103 (2024).

[17] G. Rumi, J. A. Sánchez, F. Elías, R. C. Maldonado, J. Puig, N. R. C. Bolecek, G. Nieva, M. Konczykowski, Y. Fasano, and A. B. Kolton, Hyperuniform vortex patterns at the surface of type-II superconductors, Phys. Rev. Res. **1**, 033057 (2019).

[18] J. Aragón Sánchez, R. Cortés Maldonado, N. R. Cejas Bolecek, G. Rumi, P. Pedrazzini, M. I. Dolz, G. Nieva, C. J. v. d. Beek, M. Konczykowski, C. D. Dewhurst, R. Cubitt, A. B. Kolton, A. Pautrat, and Y. Fasano, Unveiling the vortex glass phase in the surface and volume of a type-II superconductor, Commun. Phys. **2**, 143 (2019).

[19] D. Chen, R. Samajdar, Y. Jiao, and S. Torquato, Anomalous suppression of large-scale density fluctuations in classical and quantum spin liquids, Proc. Natl. Acad. Sci. USA **122**, e2416111122 (2025).

[20] Q.-L. Lei, M. P. Ciamarra, and R. Ni, Nonequilibrium strongly hyperuniform fluids of circle active particles with large local density fluctuations, Sci. Adv. **5**, eaau7423 (2019).

[21] Y. Zheng, M. A. Klatt, and H. Löwen, Universal hyperuniformity in active field theories, Phys. Rev. Res. **6**, L032056 (2024).

[22] E. C. Oğuz, J. E. S. Socolar, P. J. Steinhardt, and S. Torquato, Hyperuniformity of quasicrystals, Phys. Rev. B **95**, 054119 (2017).

[23] S. Torquato, G. Zhang, and M. de Courcy-Ireland, Hidden multiscale order in the primes, J. Phys. A: Math. Theor. **52**, 135002 (2019).

[24] O. H. E. Philcox and S. Torquato, Disordered heterogeneous universe: Galaxy distribution and clustering across length scales, Phys. Rev. X **13**, 011038 (2023).

[25] More generally, it is one in which the local number variance $\sigma^2(R)$ (defined in Sec. II A) grows more slowly than $R^d$ for large $R$. This definition applies even when $S(k)$ is not continuous as $k$ tends to zero, such as for quasicrystals [22] or the prime numbers [23].

[26] O. U. Uche, F. H. Stillinger, and S. Torquato, Constraints on collective density variables: Two dimensions, Phys. Rev. E **70**, 046122 (2004).

[27] R. D. Batten, F. H. Stillinger, and S. Torquato, Classical disordered ground states: Super-ideal gases, and stealth and equi-luminous materials, J. Appl. Phys. **104**, 033504 (2008).

[28] S. Torquato, G. Zhang, and F. H. Stillinger, Ensemble theory for stealthy hyperuniform disordered ground states, Phys. Rev. X **5**, 021020 (2015).

[29] L. S. Froufe-Pérez, M. Engel, P. F. Damasceno, N. Muller, J. Haberko, S. C. Glotzer, and F. Scheffold, Role of short-range order and hyperuniformity in the formation of band gaps in disordered photonic materials, Phys. Rev. Lett. **117**, 053902 (2016).

[30] L. S. Froufe-Pérez, M. Engel, J. J. Sáenz, and F. Scheffold, Band gap formation and Anderson localization in disordered photonic materials with structural correlations, Proc. Natl. Acad. Sci. USA **114**, 9570 (2017).

[31] L. Siedentop, G. Lui, G. Maret, P. M. Chaikin, P. J. Steinhardt, S. Torquato, P. Keim, and M. Florescu, Stealthy and hyperuniform isotropic photonic band gap structure in 3D, PNAS Nexus **3**, 383 (2024).

[32] G. Gkantzounis, T. Amoah, and M. Florescu, Hyperuniform disordered phononic structures, Phys. Rev. B **95**, 094120 (2017).

[33] V. Romero-García, N. Lamothe, G. Theocharis, O. Richoux, and L. M. García-Raffi, Stealth acoustic materials, Phys. Rev. Appl. **11**, 054076 (2019).

[34] L. Alhaïtz, J.-M. Conoir, and T. Valier-Brasier, Experimental evidence of isotropic transparency and complete band gap formation for ultrasound propagation in stealthy hyperuniform media, Phys. Rev. E **108**, 065001 (2023).

[35] T. Ma, H. Guerboukha, M. Girard, A. D. Squires, R. A. Lewis, and M. Skorobogatiy, 3D printed hollow-core terahertz optical waveguides with hyperuniform disordered dielectric reflectors, Adv. Opt. Mater. **4**, 2085 (2016).

[36] B.-Y. Wu, X.-Q. Sheng, and Y. Hao, Effective media properties of hyperuniform disordered composite materials, PLoS ONE **12**, e0185921 (2017).

[37] J. Kim and S. Torquato, Theoretical prediction of the effective dynamic dielectric constant of disordered hyperuniform

anisotropic composites beyond the long-wavelength regime, Opt. Mater. Express **14**, 194 (2024).
[38] J. Kim and S. Torquato, Extraordinary optical and transport properties of disordered stealthy hyperuniform two-phase media, J. Phys.: Condens. Matter **36**, 225701 (2024).
[39] G. Zhang, F. H. Stillinger, and S. Torquato, Transport, geometrical and topological properties of stealthy disordered hyperuniform two-phase systems, J. Chem. Phys **145**, 244109 (2016).
[40] G. Zhang, F. H. Stillinger, and S. Torquato, Can exotic disordered "stealthy" particle configurations tolerate arbitrarily large holes? Soft Matter **13**, 6197 (2017).
[41] D. Chen and S. Torquato, Designing disordered hyperuniform two-phase materials with novel physical properties, Acta Mater. **142**, 152 (2018).
[42] S. Ghosh and J. L. Lebowitz, Generalized stealthy hyperuniform processes: Maximal rigidity and the bounded holes conjecture, Commun. Math. Phys. **363**, 97 (2018).
[43] R. D. Batten, F. H. Stillinger, and S. Torquato, Novel low-temperature behavior in classical many-particle systems, Phys. Rev. Lett. **103**, 050602 (2009).
[44] R. D. Batten, F. H. Stillinger, and S. Torquato, Interactions leading to disordered ground states and unusual low-temperature behavior, Phys. Rev. E **80**, 031105 (2009).
[45] J. Park, S. Park, K. Kim, J. Kwak, S. Yu, and N. Park, Deep-subwavelength engineering of stealthy hyperuniformity, Nanophotonics **14**, 1113 (2025).
[46] O. U. Uche, S. Torquato, and F. H. Stillinger, Collective coordinates control of density distributions, Phys. Rev. E **74**, 031104 (2006).
[47] G. Zhang, F. H. Stillinger, and S. Torquato, Ground states of stealthy hyperuniform potentials: I. Entropically favored configurations, Phys. Rev. E **92**, 022119 (2015).
[48] G. Zhang, F. H. Stillinger, and S. Torquato, Ground states of stealthy hyperuniform potentials: II. Stacked-slider phases, Phys. Rev. E **92**, 022120 (2015).
[49] P. K. Morse, J. Kim, P. J. Steinhardt, and S. Torquato, Generating large disordered stealthy hyperuniform systems with ultrahigh accuracy to determine their physical properties, Phys. Rev. Res. **5**, 033190 (2023).
[50] P. K. Morse, P. J. Steinhardt, and S. Torquato, Ordered and disordered stealthy hyperuniform point patterns across spatial dimensions, Phys. Rev. Res. **6**, 033260 (2024).
[51] A. Sütő, From bcc to fcc: Interplay between oscillating long-range and repulsive short-range forces, Phys. Rev. B **74**, 104117 (2006).
[52] Y. Fan, J. K. Percus, D. K. Stillinger, and F. H. Stillinger, Constraints on collective density variables: One dimension, Phys. Rev. A **44**, 2394 (1991).
[53] R. B. Batten, F. H. Stillinger, and S. Torquato, Inherent structures for a soft long-range interaction in two-dimensional many-particle systems, J. Chem. Phys. **135**, 054104 (2011).
[54] S. Torquato, *Random Heterogeneous Materials: Microstructure and Macroscopic Properties* (Springer-Verlag, New York, 2002).
[55] J. P. Hansen and I. R. McDonald, *Theory of Simple Liquids* (Academic Press, New York, 1986).
[56] E. Lomba, J.-J. Weis, and S. Torquato, Disordered hyperuniformity in two-component non-additive hard disk plasmas, Phys. Rev. E **96**, 062126 (2017).
[57] C. E. Zachary and S. Torquato, Anomalous local coordination, density fluctuations, and void statistics in disordered hyperuniform many-particle ground states, Phys. Rev. E **83**, 051133 (2011).
[58] C. E. Zachary and S. Torquato, Hyperuniformity in point patterns and two-phase heterogeneous media, J. Stat. Mech. (2009) P12015.
[59] S. Torquato, Structural characterization of many-particle systems on approach to hyperuniform states, Phys. Rev. E **103**, 052126 (2021).
[60] B. Widom, Equation of state in the neighborhood of the critical point, J. Chem. Phys. **43**, 3898 (1965).
[61] L. P. Kadanoff, Scaling laws for Ising models near $T_c$, Phys. Phys. Fiz. **2**, 263 (1966).
[62] M. E. Fisher, The theory of equilibrium critical phenomena, Rep. Prog. Phys. **30**, 615 (1967).
[63] K. G. Wilson and J. Kogut, The renormalization group and the $\epsilon$ expansion, Phys. Rep. **12**, 75 (1974).
[64] J. J. Binney, N. J. Dowrick, A. J. Fisher, and M. E. J. Newman, *The Theory of Critical Phenomena: An Introduction to the Renormalization Group* (Oxford University Press, Oxford, 1992).
[65] E. C. Oğuz, J. E. S. Socolar, P. J. Steinhardt, and S. Torquato, Hyperuniformity and anti-hyperuniformity in one-dimensional substitution tilings, Acta Cryst. A: Found. Adv. **A75**, 3 (2019).
[66] R. Schneider and W. Weil, *Stochastic and Integral Geometry* (Springer, Berlin, 2008).
[67] M. A. Klatt, J. Lovrić, D. Chen, S. C. Kapfer, F. M. Schaller, P. W. A. Schönhöfer, B. S. Gardiner, A.-S. Smith, G. E. Schröder-Turk, and S. Torquato, Universal hidden order in amorphous cellular geometries, Nat. Commun. **10**, 811 (2019).
[68] C. Helgert, C. Rockstuhl, C. Etrich, E. B. Kley, A. Tünnermann, F. Lederer, and T. Pertsch, Effects of anisotropic disorder in an optical metamaterial, Appl. Phys. A **103**, 591 (2011).
[69] M. A. Klatt, J. Kim, and S. Torquato, Cloaking the underlying long-range order of randomly perturbed lattices, Phys. Rev. E **101**, 032118 (2020).
[70] A. Gabrielli, Point processes and stochastic displacement fields, Phys. Rev. E **70**, 066131 (2004).
[71] H. Wang and S. Torquato, Designer pair statistics of disordered many-particle systems with novel properties, J. Chem. Phys. **160**, 044911 (2024).
[72] B. Jancovici, Exact results for the two-dimensional one-component plasma, Phys. Rev. Lett. **46**, 386 (1981).
[73] F. H. Stillinger and D. K. Stillinger, Negative thermal expansion in the Gaussian core model, Physica A **244**, 358 (1997).
[74] C. E. Zachary, F. H. Stillinger, and S. Torquato, Gaussian-core model phase diagram and pair correlations in high Euclidean dimensions, J. Chem. Phys. **128**, 224505 (2008).
[75] M. C. Rechtsman, F. H. Stillinger, and S. Torquato, Negative thermal expansion in single-component systems with isotropic interaction, J. Phys. Chem. A **111**, 12816 (2007).
[76] G. Yatsenko, E. J. Sambriski, M. A. Nemirovskaya, and M. Guenza, Analytical soft-core potentials for macromolecular fluids and mixtures, Phys. Rev. Lett. **93**, 257803 (2004).
[77] B. Widom, Random sequential addition of hard spheres to a volume, J. Chem. Phys. **44**, 3888 (1966).
[78] J. Feder, Random sequential adsorption, J. Theor. Biol. **87**, 237 (1980).

[79] G. Zhang and S. Torquato, Precise algorithm to generate random sequential addition of hard hyperspheres at saturation, Phys. Rev. E **88**, 053312 (2013).

[80] S. Torquato, O. U. Uche, and F. H. Stillinger, Random sequential addition of hard spheres in high Euclidean dimensions, Phys. Rev. E **74**, 061308 (2006).

[81] See Supplemental Material at http://link.aps.org/supplemental/10.1103/9wbz-h7t4 for movies that show the evolution of HIP, POS, and GAU initial conditions to their respective stealthy ground states with $\chi = 0.4$. The HIP configuration takes the largest computational time to reach a stealthy ground state, followed by POS, followed by GAU which takes the least computational time to reach a ground state. The evolution of GAU to a ground state takes very little time and reflects the small configurational distance of this initial condition away from the ground-state manifold. The computational speed is the same for each initial condition.

[82] C. E. Maher and S. Torquato, Local order metrics for many-particle systems across length scales, Phys. Rev. Res. **6**, 033262 (2024).

[83] S. Yu, C.-W. Qiu, Y. Chong, S. Torquato, and N. Park, Engineered disorder in photonics, Nat. Rev. Mater. **6**, 226 (2021).